Renewable Energy 209 (2023) 122–132

Contents lists available at ScienceDirect

Renewable Energy

journal homepage: www.elsevier.com/locate/renene

Numerical analysis of the fluid flow and heat transfer of a hybrid PV-thermal collector and performance assessment

María Herrando [a,*], Guillermo Fantoni [a], Ana Cubero [a], Raquel Simón-Allué [b], Isabel Guedea [b], Norberto Fueyo [a]

[a] Fluid Dynamics Technology Group, I3A, University of Zaragoza, Zaragoza, Spain
[b] EndeF Solar Solutions, Zaragoza, Spain

ARTICLE INFO

Keywords:
Computational fluid dynamics (CFD) modelling
Fluid flow
Hybrid photovoltaic-thermal (PV-T) collector
Roll-bond thermal absorber
Energy performance modelling

ABSTRACT

In recent years, new materials and absorber configurations have been proposed to improve the performance of hybrid photovoltaic-thermal (PV-T) collectors. This work analyses the fluid flow and the energy performance of an uncovered water-based PV-T collector with a roll-bond thermal absorber. A detailed CFD model was developed and the results were compared with the experimental performance features provided by the PV-T manufacturer. The fluid flow results show uneven flow distribution among the roll-bond microchannels which leads to areas with larger PV cell temperatures and thus a lower electricity generation. The PV-T collector layers were also modelled using the energy transfer equations layer-by-layer. The model was run for several water inlet temperatures and water flow-rates to obtain the thermal performance curve. The results show that the electrical efficiency of the PV-T collector is 14.5–10.3% larger than for a PV-only system for water inlet temperatures of 20–30 °C, respectively. The developed CFD model reproduces accurately the thermal performance of the PV-T collector, with a maximum error of 6.5% for inlet water temperatures of 20–60 °C. Therefore, this model can be used with confidence to propose alternative designs that achieve a homogeneous temperature distribution in the PV layer and improve the overall PV-T collector performance.

1. Introduction

The Paris Climate Conference in 2015 [1] concluded through a legally-binding agreement signed by over 190 countries to keep the rise in the average global temperature below 2 °C (above 20th-century pre-industrial levels) [2]. Decarbonisation of the energy systems is essential to meet this ambitious target [3]. This energy transition from fossil-fuel-based systems to clean energy systems can be achieved by several parallel actions, including an increasing penetration rate of renewable energy systems, smart technologies and clean energy policies, among others [3].

Research on renewable energy systems is rapidly progressing in the last decades [4], demonstrating the techno-economic feasibility of these systems [5] to promote the security of supply while lowering energy costs, reducing greenhouse gas emissions, as well as driving growth through job generation and industrial development [6]. It is believed that solar energy can play a key role in this energy transition [7], as it is an abundant primary-energy resource, which can be exploited in several cost-competitive and reliable ways [8]. Still, more research is required in resource assessment, energy efficiency enhancement of different technologies and demand-supply integration [8].

Heating and cooling demands in buildings are mainly satisfied by fossil fuel technologies [5], while renewable energy sources such as solar [9], wind [10] or biomass [4] can be used, as shown in the literature [11]. Among the different solar technologies, hybrid photovoltaic-thermal (PV-T) collectors generate both electrical and thermal outputs from the same aperture area [12], presenting a higher overall energy output per collector area than side-by-side photovoltaic (PV) and solar thermal collectors [13]. Liquid-based PV-T collectors are the most common type of PV-T collectors used to provide heat and power in buildings [14,15], although air-based PV-T collectors are gaining attention [16], particularly as building-integrated PV-T systems [17]. The most common fluid employed is water, or a mixture of water-glycol to avoid freezing [18], as those are considered the most efficient PV-T collector type for water preheating all year long [19].

Among the different configurations, copper is the most widespread solid material used in liquid-based PV-T collectors [20], and the

* Corresponding author.
E-mail address: mherrando@itainnova.es (M. Herrando).

https://doi.org/10.1016/j.renene.2023.03.125
Received 22 December 2022; Received in revised form 17 March 2023; Accepted 28 March 2023
Available online 28 March 2023

Nomenclature

Symbols

a_1	linear heat loss coefficient (W/(m^2·K))
a_2	quadratic heat loss coefficient (W/(m^2·K^2))
A_c	PV-T absorber area (m^2)
α	absorptivity (−)
β_0	power temperature coefficient for the PV panel (%/K)
δ	thickness (m)
ε	emissivity (−)
G	solar irradiance (W/m^2)
η	PV-T efficiency (−)
h	heat transfer coefficient (W/(m^2·K))
I_{mpp}	Current at P_{max} [A]
k	thermal conductivity (W/(m·K))
P_p	Peak electrical power [W]
q	heat flux (W/m^2)
Q_u	Total heat transferred to the fluid (W)
σ	Stefan-Boltzmann constant ($\sigma = 5.67{\cdot}10^{-8}$ W/(m^2·K^4))
τ	transmittance (−)
T	temperature (K)
V_{mpp}	Voltage at P_{max} [V]
v_{wind}	wind speed (m/s)
w_e	electrical yield of the system (W/m^2)

Subscripts

a	ambient
abs	absorber
g	glass layer
in	inlet
ins	insulation layer
longλ	long wavelengths
PV	PV layer
PV,ref	reference PV panel
shortλ	short wavelengths
th	thermal
cv,b	convection of air at the back of the PV-T collector
fm	fluid mean
r	reduced
rd	radiation
ref	reference
u	useful

sheet-and-tube arrangement is the most common thermal absorber design [21]. Most of the sheet-and-tube thermal absorbers comprise parallel pipes connected in series [22] or a serpentine tube [23]; although other authors proposed web-flow [24], or spiral-flow [25] designs made of stainless steel. The main drawback of the sheet-and-tube configuration is the thermal contact between the PV cells and the thermal absorber, as in several cases the thermal absorber is directly glued with the PV cells, leading to poor thermal contact [26]. Previous research reported a 6–8% increase in electrical efficiency by improving this thermal contact, due to the reduction (by 10 °C) in the PV cell temperature [26]. In this line, several studies [27,28] concluded that the absorber plate should be in direct thermal contact with the PV cells to enhance energy performance.

In recent years, new materials and absorber configurations have been proposed to improve bonding quality [29] and heat transfer [30,31]. The enhancement of heat transfer can be achieved by increasing the thermal contact [32] area and by creating turbulence [33]. Twisted or perforated tapes, wire coils, inserts/baffle plates, grooves, or internally finned tubes have been proposed to increase turbulence [34]. However, this leads to larger pressure drops, thus increasing the pumping energy consumption and reducing the net power output [35].

The thermal contact area can be increased by reducing the pipe diameter D and increasing the number of channels per unit width (i.e., a shorter distance (W) between pipes) [36,37], which involves a lower W/D ratio. However, the costs and weight of the PV-T collector increase with the number of channels [38]. To solve this problem, several authors proposed flat-box [39], or roll-bond [40,41] structures, made of aluminium [42,43] or polycarbonate [32,44]. The flat-box structure allows for reducing the W/D ratio to 1 when square channels are used [45], improving the fin efficiency and bonding quality, and thus increasing the heat transfer area [32]. In this line, a parametric analysis [46] concluded that the collector should have a fluid layer thickness of less than 10 mm to collect more than 90% of the energy.

Some authors [47,48] reported a global efficiency of 87% in controlled conditions, with a maximum thermal efficiency of 75% [47], with an aluminium roll-bond design with a fractal shape (FracTherm® heat exchanger). Similar results were reported in another experimental analysis with a covered roll-bond PV-T collector, where 79% thermal efficiency and 8.7% electrical efficiency were measured when the mean fluid temperature is equal to the ambient temperature [49]. Recent research [50] analysed a serpentine roll-bond PV-T collector and compared its performance with alternative parallel-tube configurations (named Harp designs in the work) and with a spiral design. The numerical analysis concluded that the serpentine configuration achieves the highest thermal efficiency (46%) but the larger pressure drop reduces the net electrical power output [50]. Given the promising results of roll-bond thermal absorbers, this research analyses this type of configuration with a low W/D ratio to increase heat transfer.

The PV-T collector cover reduces thermal losses, increasing thermal efficiency [51,52], but it also reduces electrical efficiency (by up to 10–20% [26]) due to larger PV cell temperature and reflection losses [53,54]. Therefore, there is a trade-off between thermal and electrical efficiencies [55], and thus the best PV-T collector configuration depends on the needs of the specific application. Single-covered PV-T collectors seem an interesting option when a significant thermal output is needed [56], while uncovered PV-T collectors are recommended to satisfy low-temperature water demand all year-round [57] or to act as the source of a heat pump [55]. This work proposes uncovered PV-T collectors to preheat water while keeping high electrical efficiencies, lowering also the cost and weight of the collector.

Manufacturing new PV-T collector prototypes and undertaking experimental studies to analyse its performance is expensive, so a detailed theoretical model that incorporates several materials and layers is important to analyse the fluid flow and heat transfer throughout the PV-T collector, and to identify potential hot spots which might lead to an underperformance of the PV cells [26]. A previous study showed a temperature variation of up to 10 °C over the surface of a sheet-and-tube PV-T collector under normal operating conditions, which led to a 5% drop in the PV cell efficiency in the identified hot regions [58].

Several 3-D computational fluid dynamics (CFD) analyses have been performed on solar thermal collectors [59–61]. Martinopoulos et al. [62] analysed the velocity field and the channel pressure drop of a polymeric solar thermal collector. Moldovan et al. [63] proposed a triangular flat-plate solar thermal collector for its integration into the building façade. Recently, the authors optimised the thickness of the water layer in the triangular solar thermal collector [64]. The performance of a new design of a hybrid parabolic trough collector and concentrator PV absorber was also analysed using ANSYS software [65].

Fewer studies model water-based PV-T collectors using CFD techniques [66], and most of them consider copper sheet-and-tube PV-T collectors [67,68] with a serpentine design [69,70] or parallel tubes [68,71]. A recent work [32] proposed alternative designs based on

polymeric materials and a flat-box structure. The study showed the utility of this type of detailed CFD analysis, for instance, to assess not only the thermal performance of the PV-T collectors but also the thermal stresses that it suffers. Several of the above CFD studies [68] modelled in detail only one of the parallel tubes, assuming a uniform flow distribution among the tubes. Therefore, there is a lack of studies that model in detail the fluid flow and heat transfer of water-based PV-T collectors modelling the whole collector.

This work fills this gap by developing a detailed 3-D CFD model to analyse the fluid flow and the energy performance of an uncovered water-based PV-T collector with a roll-bond aluminium thermal absorber (Section 2.1 includes details of the PV-T collector and Section 2.2 summarises its main parameters). Given the geometrical complexity of the problem, a multiscale approach is adopted where the fluid flow is calculated in detail first in a single channel with a very high-resolution mesh (which is impractical to adopt in the full domain), as detailed in Section 2.3.1. Then, it is ensured that the main flow characteristics are retained when half of the full (symmetrical) channel network is simulated with a smaller mesh resolution (Section 2.3.2). And finally, the solid layers (such as the PV layer and the glass) are added to the model (Section 2.3.3). The detailed analysis of the fluid flow in the whole thermal absorber allows the detection of a non-uniform flow distribution throughout the PV-T collector (Section 3.1). The impact of such non-uniformities in the temperature distribution is then quantified, along with the associated performance loss (Section 3.2). The thermal performance curve obtained in the CFD simulation is used to validate the model against the experimental performance provided by the PV-T manufacturer (Section 3.3). Once the CFD model is validated, it can be used to study design modifications to improve the thermal and electrical performances of the PV-T collector, reducing the number of experimental analyses and their associated costs (Section 4).

2. Methodology

A 3-D CFD model has been developed in ANSYS Fluent to simulate the PV-T collector and its results are validated against an experimentally-derived performance curve provided by the collector manufacturer.

2.1. PV-T collector modelling

The PV cells and the thermal absorber are the two main components of a PV-T collector. In Fig. 1, a schematic of the collector layers is shown: glazing, PV cells, EVA and Tedlar layers, thermal absorber (fluid channels) and insulation. The thermal absorber is made of aluminium with a roll-bond design to increase the thermal contact area between the PV cells and the fluid (a water-glycol mixture).

The PV-T CFD model is developed under the following assumptions.

- radiation absorption in the glass layer and the collector frame is negligible [32,72];
- the ambient temperature is uniform around the collector [73,74] and heat losses from the frame of the PV-T collector are negligible [74];
- the PV cells and the thermal absorber are in perfect thermal contact [36];
- solar irradiance and wind speed are uniform over the collector surface area [32].

The model is run under steady-state conditions [32,52,75]. The detailed 3-D CFD model of the PV-T collector involves fluid dynamics and heat transfer. The continuity, momentum and energy equations are solved in the water channels of the absorber, and the energy conservation equation is used in the solid parts. Boundary conditions for these equations are detailed below and shown in Fig. 1.

2.1.1. Top layer

Losses through the top of the PV-T collector are mainly due to forced convection caused by wind (q_{wind}, see eq. (1) and eq. (2)), radiation from the glass to the sky ($q_{rd,sky}$, see eq. (3)) and radiation from the PV layer to the sky due to glass transmittance at long wavelengths ($q_{rd,PVsky}$, see eq. (7)) [76].

Various expressions are given in different sources for the estimation of the forced convective heat transfer coefficient (h_{wind}) [74,77–79], all of them dependent on the wind speed (v_{wind}). These correlations do not differ significantly, so it was decided to use the expression that provides intermediate values, within the range of the various predictions [32]. Hence:

$$q_{wind} = h_{wind} \cdot \left(T_g - T_a\right) \quad (1)$$

$$h_{wind} = 4.5 + 2.9 \cdot v_{wind} \quad (2)$$

The radiative heat loss to the sky, $q_{rd,sky}$, can be calculated as [80,81],

$$q_{rd,sky} = \varepsilon_{g,long\lambda} \cdot \sigma \cdot \left(T_g{}^4 - T_{sky}{}^4\right) \quad (3)$$

where $\varepsilon_{g,long\lambda}$ is the glass emissivity at long wavelengths, σ is the Stefan-Boltzmann constant ($\sigma = 5.67 \cdot 10^{-8}$ W/(m^2·K^4)), T_g is the glass temperature, and T_{sky} is the sky temperature, which is calculated as $T_{sky} = 0.0552 \cdot T_a^{1.5}$ [73,74,81], with the ambient temperature (T_a) in Kelvin.

The absorption of solar radiation by the top layer (glass) at short wavelengths is neglected, given the very low absorptivity of glass ($\alpha_{g,short\lambda} = 0.05$).

2.1.2. PV layer

The fraction of the total solar irradiance (G) that is not reflected by the glass is absorbed by the PV layer (G_{PV}). Such fraction is calculated as:

$$G_{PV} = G \cdot \tau_{g,short\lambda} \cdot \alpha_{PV,short\lambda} \quad (4)$$

where $\tau_{g,short\lambda}$ is the transmittance of the glass, $\alpha_{PV,short\lambda}$ is the absorptivity of the PV cells, both at short wavelengths (see Table 2) [81].

The electrical yield of the system per unit area, w_e, depends on the PV

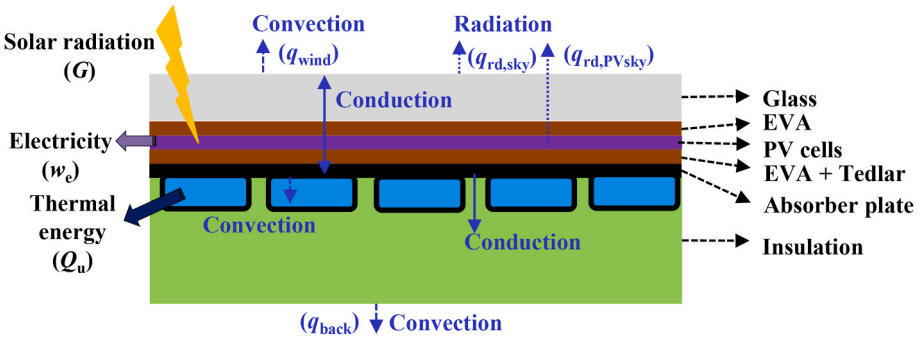

Fig. 1. PV-T collector layers and energy flows (not to scale).

Table 1
Properties of the PV panel.

Parameter/variable		Value
P_p	Peak electrical power (W)	300
V_{mpp}	Voltage at P_{max} (V)	32.5
I_{mpp}	Current at P_{max} (A)	9.25
$\eta_{PV,ref}$	Nominal PV cell efficiency (%)	18.44
β_0	Power temperature coefficient (%/K)	-0.39
-	Cell number/type (−)	60/m-Si
A_G	Gross area (m^2)	1.62
NOCT	nominal operating cell temperature (°C)	45 ± 2

panel efficiency. This term varies with temperature and can be estimated from Refs. [52,75,82]:

$$w_e = G \cdot \tau_{g,short\lambda} \cdot \eta_{PV} \quad (5)$$

$$\eta_{PV} = \eta_{PV,ref} \cdot \left[1 + \beta_0 \cdot \left(T_{PV} - T_{PV,ref}\right)\right] \quad (6)$$

where $\eta_{PV,ref}$ is the reference PV panel efficiency at a PV cell temperature $T_{PV,ref}$ of 25 °C and at a solar irradiance of 1000 W/m^2, and β_0 is the power temperature coefficient for the PV panel, values given in the technical specifications of the PV-T manufacturer.

The radiative heat loss from the PV layer to the environment, $q_{rd,PVsky}$, accounts for the radiative heat flux emitted by the PV layer at long wavelengths that is not absorbed by the glass and therefore is lost to the environment. This flux can be estimated considering the emissivity of the PV layer and the transmittance of the glass at long wavelengths as follows:

$$q_{rd,PVsky} = \tau_{g,long\lambda} \cdot \varepsilon_{PV,long\lambda} \cdot \sigma \cdot \left({T_{PV}}^4 - {T_{sky}}^4\right) \quad (7)$$

where $\tau_{g,long\lambda}$ is the transmittance of the glass and $\varepsilon_{PV,long\lambda}$ is the emissivity of the PV layer, both for long wavelengths, and T_{PV} is the temperature of the PV layer.

2.1.3. Absorber plate (roll-bond)

The heat from the PV layer to the absorber can be either transferred from the absorber layer to the cooling fluid or lost through the underside insulation layer to the environment [32,52]. The heat transfer to the absorber plate and from the absorber plate to the cooling water does not need to be imposed, as both are calculated by the CFD model, which solves the discretised energy conservation equation in these regions.

2.1.4. Back insulation layer

Since heat losses through the back insulation layer are very small, this layer is not discretised in the CFD model. Instead, the insulation layer is modelled as a resistance to heat transfer to the environment. Therefore, the heat losses, q_{back}, from the absorber plate temperature, T_{abs} (computed locally by the CFD model), to the ambient temperature, T_a, are introduced as a boundary condition:

$$q_{back} = h_{back} \cdot (T_{abs} - T_a) \quad (8)$$

where h_{back} is the heat transfer coefficient between the absorber and the environment through the back layer insulation, which is calculated as:

$$h_{back} = \frac{1}{\frac{\delta_{ins}}{k_{ins}} + \frac{1}{h_{cv,b}}} \quad (9)$$

where δ_{ins} and k_{ins} are the thickness and conductivity of the insulation layer (see Table 2), and $h_{cv,b}$ is the convective heat transfer coefficient to the air at the back (underside) of the PV-T collector, which usually takes values between 0.3 and 0.6 W/(m^2·K) [76]; an intermediate value of 0.45 W/(m^2·K) was used in the present work [32].

2.1.5. PV-T collector thermal performance

The thermal efficiency of the PV-T collector obtained in the simulation is compared with the experimental one provided by the PV-T manufacturer [83] through the thermal performance curve widely used in the literature (see eq. (10) and eq. (11)) [32,84]. Since there is currently no specific standard method to assess the performance of PV-T collectors [85], the ISO procedure approach for solar thermal collectors [86] is followed to perform the experimental characterization of the PV-T collector. This standard includes the particularization of the thermal characterization in the case of PV-T collectors, which states that the power generator (PV cells) must be kept within 15% of the module maximum power point (MPP) during the thermal testing.

$$\eta_{th} = \frac{Q_u}{G \cdot A_c} = \eta_o - a_1 \cdot T_r - a_2 \cdot G \cdot {T_r}^2 \quad (10)$$

$$T_r = \frac{T_{fm} - T_a}{G} \quad (11)$$

where Q_u is the total heat transferred to the fluid, A_c is the absorber area in direct contact with the PV panel, η_o is the optical efficiency, a_1 is the linear heat loss coefficient, a_2 is the quadratic heat loss coefficient, T_{fm} is the fluid mean temperature and T_r is the reduced temperature.

Table 2
Properties of the PV-T collector layers.

Layer	Parameter/variable		Value
Glass	δ	Thickness (m)	$3.2 \cdot 10^{-3}$
	$\varepsilon_{g,short\lambda}$	Emissivity at short wavelengths (−)	0.05
	$\tau_{g,short\lambda}$	Transmittance at short wavelengths (−)	0.94
	$\varepsilon_{g,long\lambda}$	Emissivity at long wavelengths (−)	0.86
	$\tau_{g,long\lambda}$	Transmittance at long wavelengths (−)	0.06
	k	Thermal conductivity (W/(m·K))	14
PV	$\alpha_{PV,short\lambda}$	Solar absorption coefficient at short wavelength (−)	0.95
	$\varepsilon_{PV,long\lambda}$	Emissivity at long wavelengths (−)	0.89
	δ	Thickness (m)	$3.5 \cdot 10^{-4}$
	k	Thermal conductivity (W/(m·K))	130
EVA	δ	Thickness (m)	$5 \cdot 10^{-4}$
	k	Thermal conductivity (W/(m·K))	0.35
Tedlar	δ	Thickness (m)	$3 \cdot 10^{-4}$
	k	Thermal conductivity (W/(m·K))	0.36
Absorber plate	δ	Thickness (m)	$1.5 \cdot 10^{-3}$
	k	Thermal conductivity (W/(m·K))	310
	δ	Thickness of the water layer (m)	$1.6 \cdot 10^{-3}$
Insulation	δ	Thickness (m)	0.03
	k	Thermal conductivity (W/(m·K))	0.034

2.2. PV-T collector parameters

The PV-T thermal absorber consists of a roll-bond heat exchanger in which the heat-transferring fluid (a water-glycol mixture) flows through 22 parallel aluminium channels. The PV-T collector prototype has a PV panel with a peak electrical power of 300 W_p, a nominal efficiency of 18.44%, and a power temperature coefficient (β_0) of -0.39%/K. Other PV-cell properties of interest are provided in Table 1. The nominal collector flow rate is 70 L/(m^2·h) and the thermal absorber area is 1.4 m^2. The following operating conditions are applied: a total incident solar irradiance (G) of 1000 W/m^2 and an ambient temperature (T_a) of 25 °C. The thickness, δ, and thermal conductivity, k, of the different layers as well as their optical properties are reported in Table 2.

The mains water temperature (T_{in}) is set at 20 °C for the detailed analysis of the flow distribution (Section 3.1) and the heat transfer (Section 3.2), while variations in the range of 20–70 °C are used for the model validation (Section 3.3).

2.3. CFD models

The regular geometry of the PV-T collector allows the development of several CFD models to study in detail the several aspects of fluid flow and heat transfer in the PV-T collector; these models, presented below together with their rationale, are.

i) the channel model
ii) the half-collector (fluid-only) model
iii) the half-collector model with PV-T layers.

2.3.1. Channel model

The **channel model** allows a detailed analysis of the fluid flow through one of the 22 channels in the collector (see Fig. 3 for an overview of the channels corresponding to the half-collector) using a very fine mesh. It is used to assess how the velocity develops through the channel. The mesh is refined near the walls (Fig. 2a) and has a total of 3.9 million elements.

2.3.2. Half-collector model

The **half-collector (fluid-only) model** allows for analysing how the fluid is distributed among the channels and investigating the pressure and velocity distributions in the channels. Thanks to the symmetry of the thermal absorber along the longitudinal axis, with an independent inlet and outlet on each side, only half of the PV-T collector needs to be computed. The mesh in this case has 28.8 million cells.

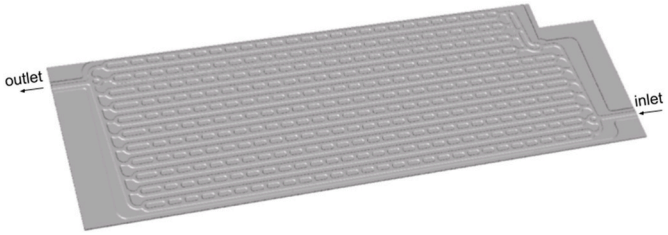

Fig. 3. Half-collector model with PV-T layers (view from the bottom of the collector, without the insulation layer).

2.3.3. Half-collector model with PV-T layers

The **half-collector model with PV-T layers** takes advantage also of the left-right symmetry of the panel to simulate only one of the two collector halves. It includes both fluid and solid regions (see Fig. 4a) so that it can be used to analyse the heat transfer through the PV-T collector. The underside insulation layer is not discretised, but represented as a heat-transfer resistance, as discussed in Section 2.1 (see Fig. 4b). Several meshes are considered using a simplified PV-T collector model (comprising only part of a channel with the corresponding layers) to analyse the influence of the mesh in the results (particularly in the fluid flow). The selected meshes for the fluid flow and the thermal absorber are tetrahedral, with refined elements near the walls (see Fig. 4a). The mesh in the upper PV-T layers is hexahedral to facilitate heat transfer convergence and reduce the number of elements. The mesh has a total of 13.1 million elements (see Fig. 4b).

3. Results and discussion

First, the fluid flow through one of the 22 channels in the PV-T collector is analysed in detail to assess how the velocity develops through the channel. Then, the fluid side of the half collector is discretised and solved (making use of the PV-T collector symmetry), to analyse the fluid distribution among the channels and to compare the results with the previous model. Finally, the PV-T layers are added to the half-collector model, discretising all of them except for the insulation layer to analyse the heat transfer through the PV-T collector, to obtain the thermal performance curve and to compare it with the experimental performance provided by the PV-T manufacturer.

3.1. Fluid flow

The velocity field in a channel is solved assuming that the fluid is uniformly distributed through the 22 channels, at the nominal flow rate (70 L/(m^2·h)). Thus, the nominal flow rate per channel is set at 4.45 L/h.

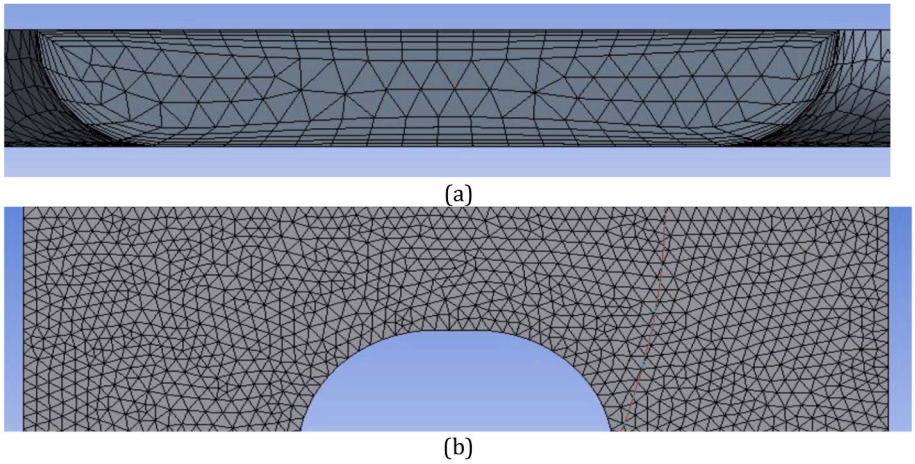

Fig. 2. (a) Transversal view of the mesh at the channel entrance and (b) mesh view from the top of the channel in the channel model.

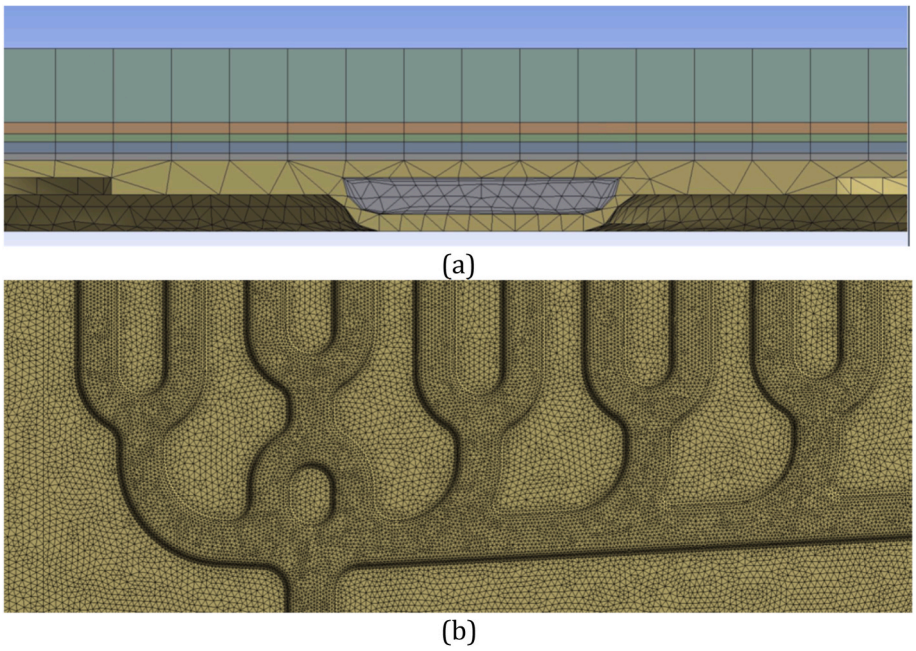

Fig. 4. (a) Transversal view of the mesh at the channel entrance and (b) mesh view (detail) from the bottom in the half-collector model with PV-T layers.

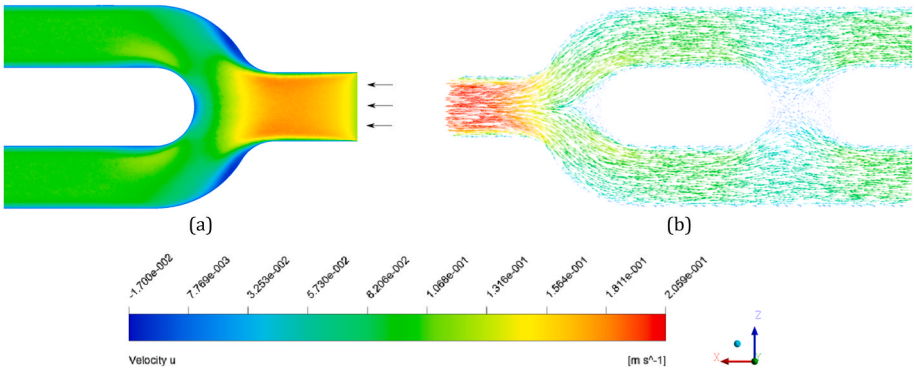

Fig. 5. (a) x-component of the velocity at the inlet and (b) velocity vectors at the outlet of a channel.

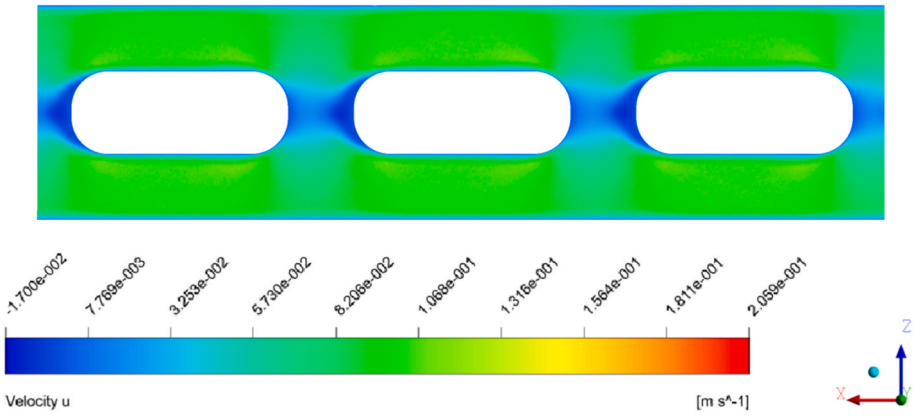

Fig. 6. x-component of the velocity in the middle region of a channel.

Considering the hydraulic diameter of each channel, the Reynolds number obtained at the inlet of each channel is 130, so the flow is modelled as laminar.

Fig. 5a shows that the fluid enters the channel and is uniformly distributed among both sub-channels. It is observed that the flow becomes fully developed in the first part of the channel and that there is no substantial flow across the passages connecting the sub-channels (see Figs. 5b and 6).

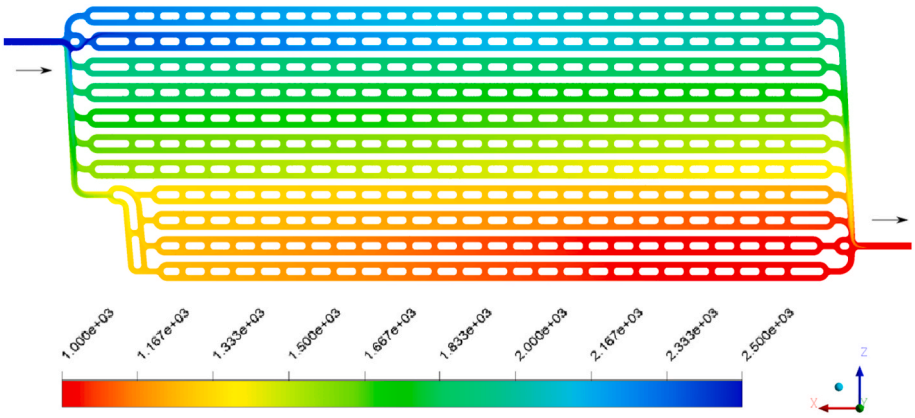

Fig. 7. Pressure field in the half-collector, fluid-only model (range 1000–2500 Pa).

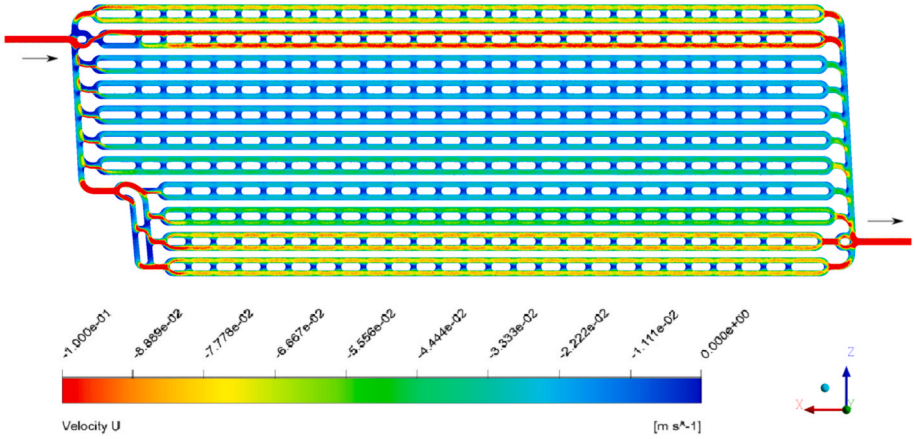

Fig. 8. Longitudinal component of the velocity in the half-collector, fluid-only model (note that velocity values are negative because the flow direction is opposite to the reference axis).

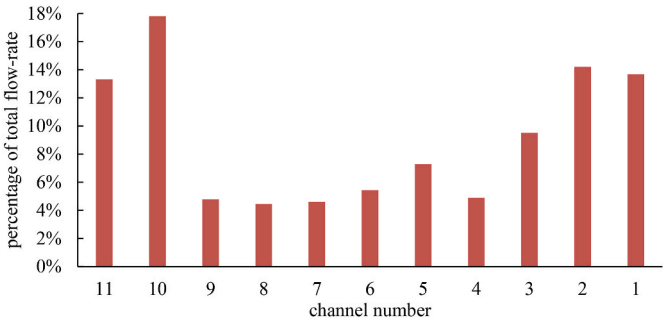

Fig. 9. Flow-rate distribution among the 11 channels of the half PV-T collector (channel 1 refers to the channel in the upper part of Fig. 8, i.e. close to the collector inlet, while channel 11 refers to the channel in the lower part, i.e. close to the collector outlet).

Although the flow distribution for the above analysis has been assumed to be uniform across the 22 channels, the fluid flow analysis of the half-collector model suggests otherwise. The Reynolds number at the entrance of the PV-T collector is 2390, so the flow is turbulent at low Re numbers. The pressure field in the half-collector, fluid-side-only model shows that there is a pressure gradient between the inlet and outlet of the collector, located in diagonally-opposed corners and that some channels experience larger pressure drops than others (see Fig. 7), leading to an uneven flow-rate distribution among the channels (see Fig. 8). Specifically, the fluid flows with a larger velocity in the channels closer to the inlet and outlet of the collector, with low velocities in the intermediate channels. The lower flow rates shown in the (7) intermediate channels lead to a decrease in the heat transfer in this area, penalising the thermal production of the absorber (see Section 3.2).

Fig. 9 shows that there is a preferential flow through the two channels close to the collector inlet (channels 1 and 2) and the two channels close to the collector outlet (channels 10 and 11), with 13–18% of the total flow rate flowing through each of these channels (in an even flow distribution, the flow rate in each channel would be 9.1% of the total). The flow rate through most of the intermediate channels is around 5% of the total. This is expected to lead to an uneven temperature distribution in the PV-T collectors.

3.2. *Heat transfer*

The flow fields obtained in the previous analysis showed that the flow distribution among the channels in the half PV-T collector is uneven. It is therefore necessary to model heat transfer in this half collector. The domain is that described in Section 2.3.3, *Half-collector model with PV-T layers*.

Fig. 10 shows that cooling-fluid temperature increase as the water moves along the several channels from left (inlet) to right (outlet). The highest water temperature is reached towards the outlet of the intermediate channels, because they have the lowest cooling flow rates, as shown in Fig. 9. The temperature increases to a lesser extent along the outer channels, resulting in lower final temperatures at the end of these channels.

The temperature distribution in the (solid) thermal absorber is shown in Fig. 11. In this case, the highest temperatures are reached at the corners of the PV-T collector, because the corners are not cooled by

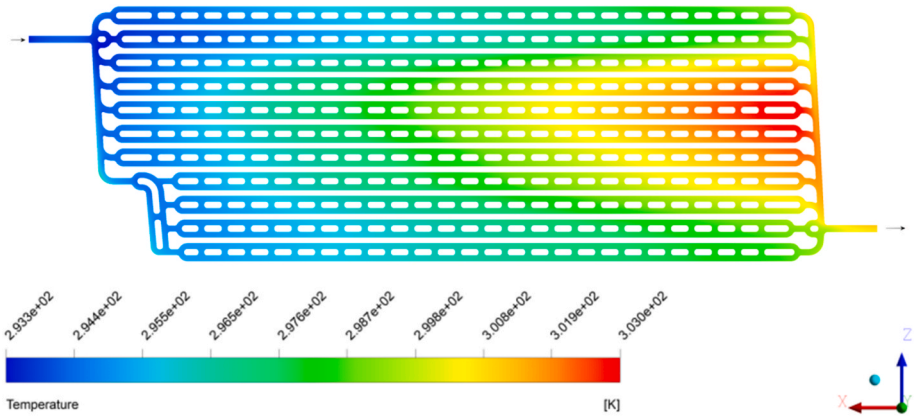

Fig. 10. Temperature distribution in the fluid through half PV-T collector.

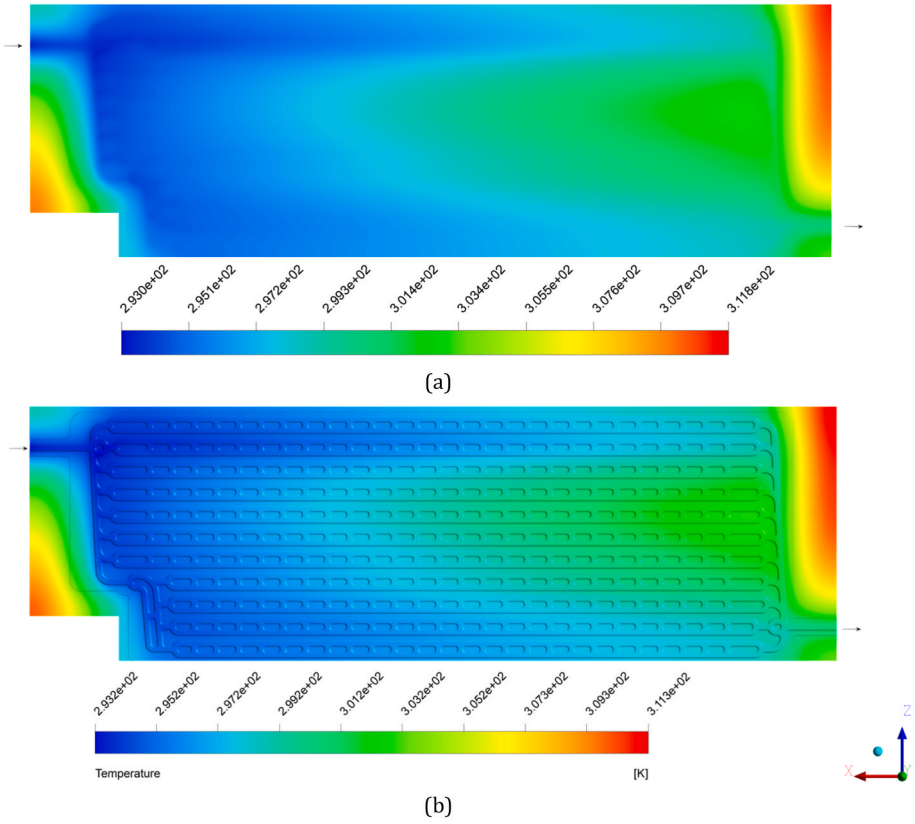

Fig. 11. Temperature distribution in the solid thermal absorber of the PV-T collector: (a) aluminium layer and (b) embossed aluminium layer.

water channels. The temperatures in the thermal absorber above the channels are also non-uniform in this PV-T collector design. This uneven temperature distribution results in less heat being transferred in the central channels of each half collector, reducing the thermal efficiency and (because of the higher temperatures) the electricity production. For instance, the temperature in the thermal absorber above channel 1 varies from 20 °C at the beginning to 27 °C at the end of the channel; in a central channel (e.g. channel 5) it varies from 21 °C to 32 °C, and it is at a temperature higher than 27 °C along more than half of the channel length. In the area without water cooling (such as the upper corner of the PV-T collector), the temperature reaches 40 °C. This entails a reduction in the PV cell efficiency of 8%, from 18.8% at the collector inlet to 17.4% at the hottest points, thus limiting the total electricity generated by the PV panel.

To achieve a uniform flow rate distribution among the channels, the pressure loss along the channel can be modified by changing each channel diameter, so that the flow rate is equilibrated and the presence of preferential channels is avoided. Alternatively, these equilibrating pressure losses can be introduced in each channel in a variety of other ways, e.g. by introducing flow restrictions in the channel.

3.3. Model validation and performance curve analysis

The developed CFD model is validated using the experimental data provided by the PV-T manufacturer, obtained under standard test conditions following the testing procedures indicated in the ISO 9806 standard [86]. To this end, the complete half-collector CFD model (with PV-T layers) is run with different fluid inlet temperatures (T_{in}), from 20 °C to 70 °C. Environmental conditions are maintained constant at the standard values indicated in the ISO 9806 standard: total solar

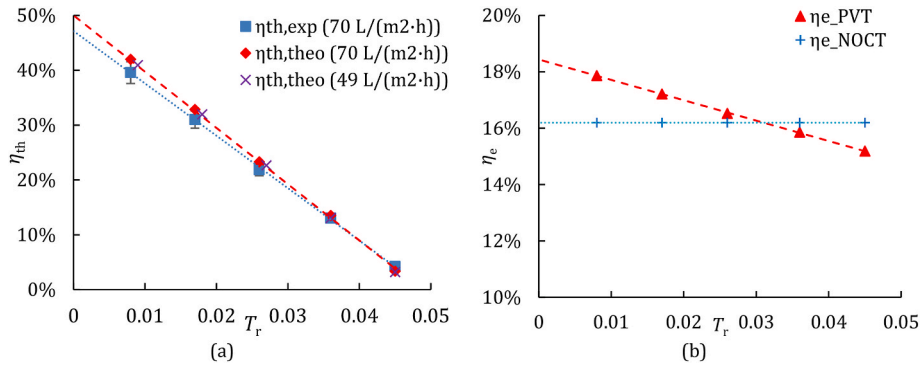

Fig. 12. (a) Experimental (exp) vs. theoretical (theo) thermal performance (η_{th}) of the PV-T collector, and (b) electrical efficiency of the PV-T collector ($\eta_{e,PVT}$) vs. electrical efficiency of a PV-only panel ($\eta_{e,NOCT}$).

irradiance (G = 1000 W/m^2), ambient temperature (T_a) of 25 °C and wind speed (v_{wind}) of 1 m/s. The nominal collector flow rate (70 L/(m^2·h)) and also 70% of the nominal collector flow rate (49 L/(m^2·h)) are considered, as this is the normal range of operation of the PV-T collector according to the manufacturer.

Results indicate a linear thermal behaviour for both flow rates, with a negligible quadratic heat loss coefficient (a_2) (see eq. (10)), in agreement with the data provided by the manufacturer. The CFD results show that the thermal efficiency varies from 51% to 3.4% for fluid inlet temperatures from 20 °C to 70 °C, for the nominal flow rate. Slightly lower results are found for the 70% flow rate, with thermal efficiencies in the range of 50–3.2%. Comparing these thermal performance results with the experimental data, Fig. 12a shows that the developed CFD model accurately reproduces the thermal performance of the PV-T collector, with a maximum error of 6.5% for T_{in} = 20–60 °C (for the nominal flow rate).

The electrical efficiency varies from 18.5% to 15.2% for fluid inlet temperatures from 20 °C to 70 °C and with the nominal flow rate (see Fig. 12b), with an average PV cell temperature varying from 24 °C to 70 °C. Similar values are obtained for the 70% flow rate, with the PV cell temperature varying from 25 °C to 70 °C and the electrical efficiency from 18.4% to 15.2%, for the same fluid inlet temperature range. These results are compared with the electrical efficiency of a PV-only panel, that is, the same PV panel without active cooling (see Fig. 12b). In this case, the PV cell temperature is estimated considering the nominal operating cell temperature (NOCT) provided by the manufacturer (see Table 1), using the following expression,

$$T_{PVcell} = T_a + G \cdot \frac{NOCT - 20}{800} \quad (12)$$

The results show that the electrical efficiency of the PV-T collector is larger than for a PV-only system for water inlet temperatures up to ~55 °C. At low water inlet temperatures (20–30 °C), typical values for normal operating conditions, the electrical efficiency is 14.5%–10.3% higher for the PV-T collector.

Table 3 shows the thermal performance parameters (η_o, optical efficiency, and a_1, heat-loss coefficient) provided by the PV-T manufacturer (experimental) and the values obtained with the CFD model (theoretical). It can be concluded that the CFD model predicts the performance of the PV-T collector satisfactorily, slightly overestimating the optical efficiency (by 5.9%) and the heat-loss coefficient (by 7.4%).

These results are in line with the findings of other research on uncovered roll-bond PV-T collectors. Bombarda et al. [87] obtained daily values of 40% thermal and 15.6% electrical efficiencies. Recent research [88] also reported similar thermal performance parameters. Colombini et al. [50] analysed three different geometries of parallel-tube configurations (named Harp designs in their work) for an uncovered roll-bond PV-T collector and reported thermal efficiencies of 39.2–44.5% and electrical efficiencies of 14.2–13.7% (depending on the geometry), for water inlet temperatures of 25 °C. The results obtained for water inlet temperatures of 45 °C were also similar to those in the present work (24.7–27.0% thermal and 12.8–13.0% electrical efficiencies). Other authors [47,89] reported thermal efficiencies of 70–75%, but for covered PV-T collectors, which achieve higher outlet water temperatures but also lower electrical efficiencies (of less than 10%) [49].

Table 3
Experimental and theoretical thermal performance parameters of the PV-T collector.

	η_o (−)	a_1 (W/(m^2·K))
Experimental	0.472	9.551
Theoretical	0.500	10.259
error (%)	*5.9%*	*7.4%*

4. Conclusion

A detailed 3-D CFD model of an uncovered water-based PV-T collector with a roll-bond aluminium thermal absorber is developed to analyse whether there is a uniform flow distribution among the absorber channels and the temperature distribution throughout the PV-T collector. The model is also validated against the experimental performance provided by the PV-T manufacturer.

The fluid flow analysis shows that there is an uneven flow distribution among the channels, which leads to an uneven temperature distribution of the PV-T collectors, as confirmed also by the CFD model of a half-collector with PV-T layers. There is a temperature difference of ~5 °C between the channels close to the collector inlet, and the intermediate channels. This uneven temperature distribution leads to a reduction of the PV cell efficiency of ~8% between the coldest and the hottest collector surface. To avoid this non-uniformity, this work proposes to modify the diameter of selected channels to increase their pressure drop (for the same flow rate), and thus, homogenise the fluid flow rate.

The results show that the thermal efficiency varies from 51% to 3.4% for fluid inlet temperatures from 20 °C to 70 °C, for the nominal flow rate. The electrical efficiency varies from 18.5% to 15.2% for the same temperature range. It is estimated that at low water inlet temperatures (20–30 °C), which are typical values for normal operating conditions, the electrical efficiency is 14.5–10.3% larger than an equivalent PV-only panel, that is, the same PV panel without active cooling. Thus, it is concluded that these PV-T collectors generate more electricity than stand-alone PV panels, along with useful thermal output.

The model validation shows that the developed CFD model accurately reproduces the thermal performance of the PV-T collector, with a maximum error of 6.5% at normal operating conditions (T_{in} = 20–60 °C). Therefore, this model can be used with confidence to propose alternative designs that achieve a homogeneous temperature distribution in the PV layer and improve the overall PV-T collector performance.

CRediT authorship contribution statement

María Herrando: Conceptualization, Methodology, Validation, Formal analysis, Investigation, Data curation, Visualization, Writing – original draft, Writing – review & editing. **Guillermo Fantoni:** Methodology, Software, Formal analysis. **Ana Cubero:** Software, Visualization. **Raquel Simón-Allué:** Data curation, Visualization, Writing – original draft. **Isabel Guedea:** Resources, Project administration, Funding acquisition. **Norberto Fueyo:** Conceptualization, Writing – review & editing, Supervision, Project administration, Funding acquisition.

Declaration of competing interest

The authors declare that they have no known competing financial interests or personal relationships that could have appeared to influence the work reported in this paper.

Data availability

Data will be made available on request.

Acknowledgements

This work was presented at the 17th Conference on Sustainable Development of Energy, Water and Environment Systems (SDEWES2022) which took place on the 6th-10th of November 2022 in Paphos (Cyprus). This work was undertaken in the framework of 3GSol, a project funded under the Retos-Colaboración 2017 Programme, National R&D and Innovation Plan, by the Spanish Government, Ministry of Science, Innovation and Universities and cofunded by the EU, through the European Regional Development Fund (ERDF) [grant number RTC-2017-6026-3]. This work was partially performed in the framework of the Juan de la Cierva Incorporación Fellowship awarded to Dr. María Herrando, funded by the Ministry of Science, Innovation and Universities (AEI) and cofounded by the EU (through the NextGeneration funds) [grant number IJC2020-043717-I].

References

[1] UNEP Climate Action, COP 21 Paris France Sustainable Innovation Forum, 2015. http://www.cop21paris.org/. (Accessed 25 June 2022).
[2] E.G. Science, Background on Impacts, Emission Pathways, Mitigation Options and Costs. The 2°C Target, Information Reference Document, 2008.
[3] P.A. Østergaard, N. Duic, Y. Noorollahi, S. Kalogirou, Latest progress in Sustainable Development using renewable energy technology, Renew. Energy 162 (2020) 1554–1562, https://doi.org/10.1016/J.RENENE.2020.09.124.
[4] P.A. Østergaard, N. Duic, Y. Noorollahi, S.A. Kalogirou, Recent advances in renewable energy technology for the energy transition, Renew. Energy 179 (2021) 877–884, https://doi.org/10.1016/J.RENENE.2021.07.111.
[5] P.A. Østergaard, N. Duic, Y. Noorollahi, S. Kalogirou, Renewable energy for sustainable development, Renew. Energy 199 (2022) 1145–1152, https://doi.org/10.1016/J.RENENE.2022.09.065.
[6] A. Carfora, R.V. Pansini, G. Scandurra, Energy dependence, renewable energy generation and import demand: are EU countries resilient? Renew. Energy 195 (2022) 1262–1274, https://doi.org/10.1016/J.RENENE.2022.06.098.
[7] Y. Noorollahi, N. Vahidrad, S. Eslami, M.N. Naseer, Modeling of transition from natural gas to hybrid renewable energy heating system, Int. J. Sustain. Energy Plan. Manag. 32 (2021) 61–78, https://doi.org/10.5278/ijsepm.6576.
[8] P.A. Østergaard, N. Duic, Y. Noorollahi, H. Mikulcic, S. Kalogirou, Sustainable development using renewable energy technology, Renew. Energy 146 (2020) 2430–2437, https://doi.org/10.1016/J.RENENE.2019.08.094.
[9] R.A. Agathokleous, S.A. Kalogirou, S. Karellas, Exergy analysis of a naturally ventilated Building Integrated Photovoltaic/Thermal (BIPV/T) system, Renew. Energy 128 (2018) 541–552, https://doi.org/10.1016/j.renene.2017.06.085.
[10] F. Calise, F.L. Cappiello, M. Dentice d'Accadia, M. Vicidomini, Dynamic modelling and thermoeconomic analysis of micro wind turbines and building integrated photovoltaic panels, Renew. Energy 160 (2020) 633–652, https://doi.org/10.1016/J.RENENE.2020.06.075.
[11] A. Buonomano, C. Forzano, S.A. Kalogirou, A. Palombo, Building-façade integrated solar thermal collectors: energy-economic performance and indoor comfort simulation model of a water based prototype for heating, cooling, and DHW production, Renew. Energy (2018), https://doi.org/10.1016/J.RENENE.2018.01.059.
[12] A. Hassan, S. Abbas, S. Yousuf, F. Abbas, N.M. Amin, S. Ali, M. Shahid Mastoi, An experimental and numerical study on the impact of various parameters in improving the heat transfer performance characteristics of a water based photovoltaic thermal system, Renew. Energy 202 (2023) 499–512, https://doi.org/10.1016/J.RENENE.2022.11.087.
[13] S.A. Kalogirou, Y. Tripanagnostopoulos, Hybrid PV/T solar systems for domestic hot water and electricity production, Energy Convers. Manag. 47 (2006) 3368–3382, https://doi.org/10.1016/j.enconman.2006.01.012.
[14] K.F. Fong, T.T. Chow, C.K. Lee, Z. Lin, L.S. Chan, Comparative study of different solar cooling systems for buildings in subtropical city, Sol. Energy 84 (2010) 227–244, https://doi.org/10.1016/J.SOLENER.2009.11.002.
[15] A. Makki, S. Omer, H. Sabir, Advancements in hybrid photovoltaic systems for enhanced solar cells performance, Renew. Sustain. Energy Rev. 41 (2015) 658–684, https://doi.org/10.1016/j.rser.2014.08.069.
[16] A.H.A. Al-Waeli, K. Sopian, H.A. Kazem, M.T. Chaichan, Photovoltaic/Thermal (PV/T) systems: status and future prospects, Renew. Sustain. Energy Rev. 77 (2017) 109–130, https://doi.org/10.1016/j.rser.2017.03.126.
[17] R.A. Agathokleous, S.A. Kalogirou, Status, barriers and perspectives of building integrated photovoltaic systems, Energy 191 (2020), 116471, https://doi.org/10.1016/j.energy.2019.116471.
[18] Y. Jia, G. Alva, G. Fang, Development and applications of photovoltaic–thermal systems: a review, Renew. Sustain. Energy Rev. 102 (2019) 249–265, https://doi.org/10.1016/j.rser.2018.12.030.
[19] R. Daghigh, M.H. Ruslan, K. Sopian, Advances in liquid based photovoltaic/thermal (PV/T) collectors, Renew. Sustain. Energy Rev. 15 (2011) 4156–4170, https://doi.org/10.1016/j.rser.2011.07.028.
[20] G.S. Menon, S. Murali, J. Elias, D.S. Aniesrani Delfiya, P.V. Alfiya, M.P. Samuel, Experimental investigations on unglazed photovoltaic-thermal (PVT) system using water and nanofluid cooling medium, Renew. Energy 188 (2022) 986–996, https://doi.org/10.1016/J.RENENE.2022.02.080.
[21] M. Herrando, A. Ramos, Photovoltaic-thermal (PV-T) systems for combined cooling, heating and power in buildings: a review, Energies 15 (2022), https://doi.org/10.3390/en15093021.
[22] M. Souliotis, N. Arnaoutakis, G. Panaras, A. Kavga, S. Papaefthimiou, Experimental study and life cycle assessment (LCA) of hybrid photovoltaic/thermal (PV/T) solar systems for domestic applications, Renew. Energy 126 (2018) 708–723, https://doi.org/10.1016/j.renene.2018.04.011.
[23] R. Santbergen, C.C.M. Rindt, H.A. Zondag, R.J.C. van Zolingen, Detailed analysis of the energy yield of systems with covered sheet-and-tube PVT collectors, Sol. Energy 84 (2010) 867–878, https://doi.org/10.1016/j.solener.2010.02.014.
[24] A. Fudholi, K. Sopian, M.H. Yazdi, M.H. Ruslan, A. Ibrahim, H.A. Kazem, Performance analysis of photovoltaic thermal (PVT) water collectors, Energy Convers. Manag. 78 (2014) 641–651, https://doi.org/10.1016/j.enconman.2013.11.017.
[25] D. Das, U. Bordoloi, A.D. Kamble, H.H. Muigai, R.K. Pai, P. Kalita, Performance investigation of a rectangular spiral flow PV/T collector with a novel form-stable composite material, Appl. Therm. Eng. 182 (2021), 116035, https://doi.org/10.1016/j.applthermaleng.2020.116035.
[26] I. Guarracino, J. Freeman, A. Ramos, S.A. Kalogirou, N.J. Ekins-Daukes, C. N. Markides, Systematic testing of hybrid PV-thermal (PVT) solar collectors in steady-state and dynamic outdoor conditions, Appl. Energy 240 (2019) 1014–1030, https://doi.org/10.1016/j.apenergy.2018.12.049.
[27] R. Zakharchenko, L. Licea-Jimeenez, S.A. Pérez-García, P. Vorobiev, U. Dehesa-Carrasco, J.F. Pérez-Robles, J. González-Hernández, Y. Vorobiev, Photovoltaic solar panel for a hybrid PV/thermal system, Sol. Energy Mater. Sol. Cells 82 (2004) 253–261, https://doi.org/10.1016/j.solmat.2004.01.022.
[28] T.T. Chow, Performance analysis of photovoltaic-thermal collector by explicit dynamic model, Sol. Energy 75 (2003) 143–152, https://doi.org/10.1016/j.solener.2003.07.001.
[29] T.T. Chow, A.L.S. Chan, K.F. Fong, Z. Lin, W. He, J. Ji, Annual performance of building-integrated photovoltaic/water-heating system for warm climate application, Appl. Energy 86 (2009) 689–696, https://doi.org/10.1016/j.apenergy.2008.09.014.
[30] L. Liu, J. Niu, J.Y. Wu, Improving energy efficiency of photovoltaic/thermal systems by cooling with PCM nano-emulsions: an indoor experimental study, Renew. Energy 203 (2023) 568–582, https://doi.org/10.1016/J.RENENE.2022.12.090.
[31] R. Liang, J. Zhang, L. Ma, Y. Li, Performance evaluation of new type hybrid photovoltaic/thermal solar collector by experimental study, Appl. Therm. Eng. 75 (2015) 487–492, https://doi.org/10.1016/j.applthermaleng.2014.09.075.
[32] M. Herrando, A. Ramos, I. Zabalza, C.N. Markides, A comprehensive assessment of alternative absorber-exchanger designs for hybrid PVT-water collectors, Appl. Energy 235 (2019) 1583–1602, https://doi.org/10.1016/J.APENERGY.2018.11.024.
[33] A. Shahsavar, P. Jha, Experimental investigation of the usability of the rifled serpentine tube to improve energy and exergy performances of a nano fluid-based photovoltaic/thermal system, Renew. Energy 170 (2021), https://doi.org/10.1016/j.renene.2021.01.117.
[34] G. Wang, Y. Zhao, Z. Quan, J. Tong, Application of a multi-function solar-heat pump system in residential buildings, Appl. Therm. Eng. 130 (2018) 922–937, https://doi.org/10.1016/j.applthermaleng.2017.10.046.
[35] S. Suman, M.K. Khan, M. Pathak, Performance enhancement of solar collectors - a review, Renew. Sustain. Energy Rev. 49 (2015) 192–210, https://doi.org/10.1016/j.rser.2015.04.087.
[36] J. Ji, J. Han, T.T. Chow, H. Yi, J. Lu, W. He, W. Sun, Effect of fluid flow and packing factor on energy performance of a wall-mounted hybrid photovoltaic/water-

heating collector system, Energy Build. 38 (2006) 1380–1387, https://doi.org/10.1016/j.enbuild.2006.02.010.
[37] T. Bergene, O.M. Lovvik, Model calculations on a flat-plate solar heat collector with integrated solar cells, Sol. Energy 55 (1995) 453–462, https://doi.org/10.1016/0140-6701(96)88784-4.
[38] N. Aste, C. del Pero, F. Leonforte, Water flat plate PV-thermal collectors: a review, Sol. Energy 102 (2014) 98–115, https://doi.org/10.1016/j.solener.2014.01.025.
[39] O. Rejeb, L. Gaillard, S. Giroux-Julien, C. Ghenai, A. Jemni, M. Bettayeb, C. Menezo, Novel solar PV/Thermal collector design for the enhancement of thermal and electrical performances, Renew. Energy 146 (2020) 610–627, https://doi.org/10.1016/j.renene.2019.06.158.
[40] M. Herrando, R. Simón, I. Guedea, N. Fueyo, The challenges of solar hybrid PVT systems in the food processing industry, Appl. Therm. Eng. (2020), 116235, https://doi.org/10.1016/j.applthermaleng.2020.116235.
[41] N. Aste, C. Del Pero, R.S. Adhikari, G. Marenzi, Effectiveness and weaknesses of supporting policies for solar thermal systems—a case-study, Sustain. Cities Soc. 14 (2015) 146–153, https://doi.org/10.1016/j.scs.2014.09.003.
[42] M. Herrando, D. Elduque, C. Javierre, N. Fueyo, Life Cycle Assessment of solar energy systems for the provision of heating, cooling and electricity in buildings: a comparative analysis, Energy Convers. Manag. 257 (2022), 115402, https://doi.org/10.1016/j.enconman.2022.115402.
[43] W. He, T. Chow, J. Ji, J. Lu, G. Pei, Hybrid photovoltaic and thermal solar-collector designed for natural circulation of water, Appl. Energy 83 (2006) 199–210, https://doi.org/10.1016/j.apenergy.2005.02.007.
[44] C. Cristofari, J. Canaletti, G. Notton, C. Darras, Innovative patented PV/TH Solar Collector: optimization and performance evaluation, Energy Proc. 14 (2012) 235–240.
[45] B.J. Huang, T.H. Lin, W.C. Hung, F.S. Sun, Performance evaluation of solar photovoltaic/thermal systems, Sol. Energy 70 (2001) 443–448.
[46] C. Cristofari, G. Notton, P. Poggi, A. Louche, Modelling and performance of a copolymer solar water heating collector, Sol. Energy 72 (2002) 99–112, https://doi.org/10.1016/S0038-092X(01)00092-5.
[47] H. Pierrick, M. Christophe, G. Leon, D. Patrick, Dynamic numerical model of a high efficiency PV-T collector integrated into a domestic hot water system, Sol. Energy 111 (2015) 68–81, https://doi.org/10.1016/j.solener.2014.10.031.
[48] Y. Bai, T.T. Chow, C. Ménézo, P. Dupeyrat, Analysis of a hybrid PV/thermal solar-assisted heat pump system for sports center water heating application, Int. J. Photoenergy 2012 (2012), https://doi.org/10.1155/2012/265838.
[49] P. Dupeyrat, C. Ménézo, H. Wirth, M. Rommel, Improvement of PV module optical properties for PV-thermal hybrid collector application, Sol. Energy Mater. Sol. Cells 95 (2011) 2028–2036, https://doi.org/10.1016/j.solmat.2011.04.036.
[50] R. Colombini, L. Molinaroli, R. Simonetti, L.P.M. Colombo, G. Manzolini, Numerical analysis of different designs of roll-bond absorber on PV/T module and performance assessment, Appl. Therm. Eng. 192 (2021), 116873, https://doi.org/10.1016/j.applthermaleng.2021.116873.
[51] P. Dupeyrat, C. Ménézo, S. Fortuin, Study of the thermal and electrical performances of PVT solar hot water system, Energy Build. 68 (2014) 751–755, https://doi.org/10.1016/j.enbuild.2012.09.032.
[52] H.A. Zondag, D.W. de Vries, W.G.J. van Helden, R.J.C. van Zolingen, A.A. van Steenhoven, The yield of different combined PV-thermal collector designs, Sol. Energy 74 (2003) 253–269, https://doi.org/10.1016/S0038-092X(03)00121-X.
[53] P. Affolter, W. Eisenmann, H. Fechner, M. Rommel, A. Schaap, H. Sorensen, Y. Tripanagnostopoulos, H. Zondag, PVT roadmap: a European guide for the development and market introduction of PV-Thermal technology, Present, in: 20th Eur. Photovolt. Sol. Energy Conf. Exhib, vol. 6, 2005, p. 10. http://www.ecn.nl/publications/default.aspx?nr=rx05170.
[54] Y. Tripanagnostopoulos, M. Souliotis, Application Aspects of Hybrid PV/T Solar Systems, 2002.
[55] M. Herrando, A. Coca-ortegón, I. Guedea, N. Fueyo, in: Experimental Study of a Solar System Based on Hybrid PVT Collectors for the Provision of Heating, Cooling and Electricity in Non-residential Buildings, 16th Conf. Sustain. Dev. Energy, Water Environ. Syst. SDEWES2021.0062, Dubrovnik, 2021.
[56] X. Tian, J. Wang, C. Wang, J. Ji, Comparison analysis of the glazed and unglazed curved water-based PV/T roofs in the non-heating season, Renew. Energy 205 (2023) 899–917, https://doi.org/10.1016/J.RENENE.2023.02.019.
[57] T.T. Chow, A review on photovoltaic/thermal hybrid solar technology, Appl. Energy 87 (2010) 365–379, https://doi.org/10.1016/j.apenergy.2009.06.037.
[58] I. Guarracino, A. Mellor, N.J. Ekins-Daukes, C.N. Markides, Dynamic coupled thermal-and-electrical modelling of sheet-and-tube hybrid photovoltaic/thermal (PVT) collectors, Appl. Therm. Eng. 101 (2016) 778–795, https://doi.org/10.1016/j.applthermaleng.2016.02.056.
[59] L.A. Tagliafico, F. Scarpa, M. De Rosa, Dynamic thermal models and CFD analysis for flat-plate thermal solar collectors – a review, Renew. Sustain. Energy Rev. 30 (2014) 526–537, https://doi.org/10.1016/j.rser.2013.10.023.
[60] M. Selmi, M.J. Al-Khawaja, A. Marafia, Validation of CFD simulation for flat plate solar energy collector, Renew. Energy 33 (2008) 383–387, https://doi.org/10.1016/j.renene.2007.02.003.
[61] D. Henderson, H. Junaidi, T. Muneer, T. Grassie, J. Currie, Experimental and CFD investigation of an ICSSWH at various inclinations, Renew. Sustain. Energy Rev. 11 (2007) 1087–1116, https://doi.org/10.1016/j.rser.2005.11.003.
[62] G. Martinopoulos, D. Missirlis, G. Tsilingiridis, K. Yakinthos, N. Kyriakis, CFD modeling of a polymer solar collector, Renew. Energy 35 (2010) 1499–1508, https://doi.org/10.1016/j.renene.2010.01.004.
[63] I. Visa, M. Moldovan, A. Duta, Novel triangle flat plate solar thermal collector for facades integration, Renew. Energy 143 (2019) 252–262, https://doi.org/10.1016/j.renene.2019.05.021.
[64] M. Moldovan, I. Rusea, I. Visa, Optimising the thickness of the water layer in a triangle solar thermal collector, Renew. Energy 173 (2021) 381–388, https://doi.org/10.1016/j.renene.2021.03.145.
[65] B. Stanek, K. Grzywnowicz, Ł. Bartela, D. Węcel, W. Uchman, A system analysis of hybrid solar PTC-CPV absorber operation, Renew. Energy 174 (2021) 635–653, https://doi.org/10.1016/j.renene.2021.04.110.
[66] A. Nahar, M. Hasanuzzaman, N.A. Rahim, S. Parvin, Numerical investigation on the effect of different parameters in enhancing heat transfer performance of photovoltaic thermal systems, Renew. Energy 132 (2019) 284–295, https://doi.org/10.1016/j.renene.2018.08.008.
[67] C.D. Corbin, Z.J. Zhai, Experimental and numerical investigation on thermal and electrical performance of a building integrated photovoltaic-thermal collector system, Energy Build. 42 (2010) 76–82, https://doi.org/10.1016/j.enbuild.2009.07.013.
[68] D. Moreno, M. Fernandez, P.M. Esquivias, A comparison of closed-form and finite-element solutions for heat transfer in a nearly horizontal, unglazed flat plate PVT water collector: performance assessment, Sol. Energy 141 (2017) 11–24, https://doi.org/10.1016/j.solener.2016.11.015.
[69] J. Zhou, H. Ke, X. Deng, Experimental and CFD investigation on temperature distribution of a serpentine tube type photovoltaic/thermal collector, Sol. Energy 174 (2018) 735–742, https://doi.org/10.1016/j.solener.2018.09.063.
[70] A. Khelifa, K. Touafek, H. Ben Moussa, I. Tabet, Modeling and detailed study of hybrid photovoltaic thermal (PV/T) solar collector, Sol. Energy 135 (2016) 169–176, https://doi.org/10.1016/j.solener.2016.05.048.
[71] S.R. Maadi, M. Khatibi, E. Ebrahimnia-Bajestan, D. Wood, Coupled thermal-optical numerical modeling of PV/T module – combining CFD approach and two-band radiation DO model, Energy Convers. Manag. 198 (2019), 111781, https://doi.org/10.1016/j.enconman.2019.111781.
[72] R.K. Agarwal, H.P. Garg, Study of a Photovoltaic-Thermal system - thermosyphonic solar water heater combined with solar cells, Energy Convers. Manag. 35 (1994) 605–620.
[73] C. Cristofari, G. Notton, J.L. Canaletti, Thermal behavior of a copolymer PV/Th solar system in low flow rate conditions, Sol. Energy 83 (2009) 1123–1138, https://doi.org/10.1016/j.solener.2009.01.008.
[74] G. Notton, C. Cristofari, M. Mattei, P. Poggi, Modelling of a double-glass photovoltaic module using finite differences, Appl. Therm. Eng. 25 (2005) 2854–2877, https://doi.org/10.1016/j.applthermaleng.2005.02.008.
[75] A. Tiwari, M.S. Sodha, Performance evaluation of solar PV/T system: an experimental validation, Sol. Energy 80 (2006) 751–759, https://doi.org/10.1016/j.solener.2005.07.006.
[76] S.A. Kalogirou, Solar Energy Engineering: Processes and Systems, second ed., Academic Press, 2014 https://doi.org/10.1016/B978-0-12-374501-9.00014-5.
[77] O. Rejeb, H. Dhaou, A. Jemni, Parameters effect analysis of a photovoltaic thermal collector: case study for climatic conditions of Monastir, Tunisia, Energy Convers. Manag. 89 (2015) 409–419, https://doi.org/10.1016/j.enconman.2014.10.018.
[78] P.J. Lunde, Solar Thermal Engineering: Space Heating and Hot Water Systems, John Wiley and Sons, Inc., New York, NY, United States, 1980.
[79] S. Bhattarai, J. Oh, S. Euh, G. Krishna, D. Hyun, Simulation and model validation of sheet and tube type photovoltaic thermal solar system and conventional solar collecting system in transient states, Sol. Energy Mater. Sol. Cells 103 (2012) 184–193, https://doi.org/10.1016/j.solmat.2012.04.017.
[80] F.P. Incropera, D.P. DeWitt, T.L. Bergman, A.S. Lavine, Fundamentals of Heat and Mass Transfer, sixth ed., John Wiley & Sons, 2007 https://doi.org/10.1016/j.applthermaleng.2011.03.022.
[81] J.A. Duffie, W.A. Beckman, W.M. Worek, Solar Engineering of Thermal Processes, John Wiley & Sons, 1974, https://doi.org/10.1115/1.2930068.
[82] E. Skoplaki, J.A. Palyvos, On the temperature dependence of photovoltaic module electrical performance: a review of efficiency/power correlations, Sol. Energy 83 (2009) 614–624, https://doi.org/10.1016/j.solener.2008.10.008.
[83] Endef solar solutions. http://endef.com, 15/11/2022.
[84] J. Antonanzas, A. del Amo, A. Martinez-Gracia, A.A. Bayod-Rujula, F. Antonanzas-Torres, Towards the optimization of convective losses in photovoltaic–thermal panels, Sol. Energy 116 (2015) 323–336, https://doi.org/10.1016/j.solener.2015.04.013.
[85] J. Allan, Z. Dehouche, S. Stankovic, L. Mauricette, Performance testing of thermal and photovoltaic thermal solar collectors, Energy Sci. Eng. 3 (2015) 310–326, https://doi.org/10.1002/ese3.75.
[86] ISO/TC 180, ISO 9806:2013 - Solar Energy. Solar Thermal Collectors, Test Methods, 2014. https://www.iso.org/standard/59879.html.
[87] P. Bombarda, G. Di Marcoberardino, A. Lucchini, S. Leva, G. Manzolini, L. Molinaroli, F. Pedranzini, R. Simonetti, Thermal and electric performances of roll-bond flat plate applied to conventional PV modules for heat recovery, Appl. Therm. Eng. 105 (2016) 304–313, https://doi.org/10.1016/j.applthermaleng.2016.05.172.
[88] R. Simón-Allué, I. Guedea, A. Coca-Ortegón, R. Villén, G. Brun, Performance evaluation of PVT panel with phase change material: experimental study in lab testing and field measurement, Sol. Energy 241 (2022) 738–751, https://doi.org/10.1016/j.solener.2022.05.035.
[89] S. Brötje, M. Kirchner, F. Giovannetti, Performance and heat transfer analysis of uncovered photovoltaic-thermal collectors with detachable compound, Sol. Energy 170 (2018) 406–418, https://doi.org/10.1016/j.solener.2018.05.030.